Aquacultural Engineering 96 (2022) 102223

Contents lists available at ScienceDirect

Aquacultural Engineering

journal homepage: www.elsevier.com/locate/aque

Comparative study of circular and square gravity-based fish cages with different dimensions under pure current conditions

Magnus Aske Mjåtveit [a], Hui Cheng [a,*], Muk Chen Ong [a], Jihoon Lee [b]

[a] Department of Mechanical and Structural Engineering and Materials Science, University of Stavanger, 4036, Stavanger, Norway
[b] Department of Marine Production Management, Chonnam National University, 50 Daehak-ro, Yeosu Jeollanam-Do 59626, Republic of Korea

ARTICLE INFO

Keywords:
Gravity type fish cage
Circular cage
Square cage
Drag force
Cultivation volume
Cage deformation

ABSTRACT

Two typical gravity-based fish cages with circular and square shapes are modeled in the present study to compare their cage deformations, cultivation volumes and drag forces under different pure current conditions. Two hydrodynamic models, *i.e.*, Morison model and Screen model, are implemented into a general finite element (FE) solver Code_Aster as a new module and employed in the dynamic analyses of the fish cages. Different cage dimensions (*i.e.*, circumferences and design heights) and current velocities are considered in the comparative study. The numerical results indicate that given the same area of netting, the circular cage can gain more cultivation volume than the square cage, especially when the initial cage volume is larger than 100,000 m^3. The square cage has a slightly larger drag force per cultivation volume than the circular cage. This study suggests that the circular cage is superior to the square fish cage for large-scale fish farms.

1. Introduction

Aquaculture is one of the most rapid-growing food production industries in the world. In 2016, aquaculture accounted for 47% of global fish production (Food and Agriculture Organization, 2020). The expanding global population together with stagnation in capture fisheries is driving the food demand from aquaculture. One way of meeting this food demand is to explore the offshore area for more suitable farming sites. The other way is to enlarge fish cages in the present sites and increase the cultivation volume per cage.

Although repositioning of fish farms at exposed sites is becoming a new trend in recent years, the strong currents and rough waves can cause a severe problem with fish welfare and may hinder this trend (Hvas et al., 2021). For Atlantic salmon (*Salmo salar*), 0.2–0.5 m/s is the optimal current velocity, and 0.75 m/s is the maximum recommended current velocity (Jónsdóttir et al., 2019; Cardia and Lovatelli, 2015). When a fish farm moves to an offshore site, the cultured fish may easily become fatigued and get stuck on the cage wall, leading to unacceptable fish welfare (Brizzi and Sabbagh, 2021). Moreover, the structural design for offshore fish farms is still in its infancy with only a few successful cases, such as Ocean Farm 1 and Havfarm (Jin et al., 2021; Li et al., 2019). Hence, it is important to derivate an optimum cage design in order to improve the capacity of the present fish cages (Shainee et al., 2013).

Throughout past decades, considerable researchers have investigated hydrodynamic forces and cage deformations of various cage shapes and mesh types. Theret (1993) successfully created software for calculating the hydrodynamic forces and the corresponding shapes of a trawl exposed to a constant flow velocity. A Finite Element (FE) solver was proposed by Tsukrov et al. (2003) to investigate the structural responses of net panels subjected to environmental loading. Endresen and Klebert (2020) compared experimental and simulated loads and responses on flexible conical and cylindrical fish cages, where the numerical results underestimated the drag forces. Balash et al. (2009) concluded from experiments that drag coefficients for nets and cylinders are similar and just modified by a function of solidity (*Sn*). Tsukrov et al. (2011) found through experiments that it is not sufficient to predict the drag coefficients of net panels only by *Sn*. By conducting experiments with cruciform and sphere structure, Lader et al. (2014) proposed that the geometry of the knot in a net structure have a major impact on the drag force. Tang et al. (2018) found that Reynolds number (*Re*), *Sn*, attack angle, knot type and twine construction are all related to the hydrodynamic coefficient of netting panels. However, these parameters are difficult to implement in numerical models completely. Thus, secondary parameters are ignored in order to make the numerical solver feasible. Cheng et al. (2020) systematically reviewed the previous

* Corresponding author.
E-mail address: hui.cheng@uis.no (H. Cheng).

https://doi.org/10.1016/j.aquaeng.2021.102223
Received 19 September 2021; Received in revised form 9 December 2021; Accepted 11 December 2021
Available online 14 December 2021

hydrodynamic models for calculating hydrodynamic forces on nets, and implement these models into a general FE solver, Code_Aster, for dynamic analyses of fish cages. The present study is performed based on the work by Cheng et al. (2020).

The most widely used fish cage shapes in Norwegian waters are either circular or square and are illustrated in Fig. 1 (AKVA Group, 2020). Previously, square fish cages were the dominant shape for fish farms, while circular fish cages are currently trending. Since circular and square fish cages are widely implemented in Norwegian fish farms, these two cage shapes are chosen in this study. In general, different types of weight systems can be applied to a fish cage to control net deformation when fish cages are subjected to strong currents. According to Cardia and Lovatelli (2015), the commonly used weight systems are (1) multiple-sinker weight system (multiple sinkers attached to floating collars using side ropes), (2) single-sinker weight system (only one single weight attached to the bottom net) and (3) sinker tube (one continuous pipe attached to the bottom net). Huang et al. (2007) found through experiments that the difference of volume reductions for the fish cages using multiple-sinker weight system and sinker tube are within 10%. In practice, the selection of weight systems depends on net material, cage shape and environmental conditions. Because the multiple weight is commonly used in conventional fish cages, it is chosen to be the studied weight system in this study.

Fish cages can be enlarged in the horizontal or vertical direction to accommodate more fish. However, a comprehensive study of gravity fish cages with different dimensions is still lacking. Li et al. (2006), Lee et al. (2008), Moe-Føre et al. (2016), Huang et al. (2006), Zhao et al. (2007a), Chen et al., (2021) and Zhao et al. (2007b) studied the effects of mesh types, submerged weights and cage sizes on the net deformations using the lumped mass model. However, these studies can hardly be applied to the aquaculture industry because (1) their model did not include the bottom nets and (2) their model-scale studies failed to reflect the hydrodynamic responses of full-scale cages (Ruzzo et al., 2021). To the authors' knowledge, no researcher has systematically compared the hydrodynamic characterizes of different types of fish cage shapes with various dimensions and current velocities. In the present study, two shapes of gravity type fish cage with varying dimensions (including circumference, design height) are modeled using a FE solver, Code_Aster. The detailed descriptions of the fish cages and their modeling method are presented in Sections 2 and 3. The effects of varying design parameters on the cage deformation, cultivation volumes and drag forces are discussed in Section 4. An insight towards the design direction for improving the cultivation volume per cage is given together with conclusions in Section 5.

2. Description of the fish cage models

In the present study, two typical Norwegian fish cages are numerically modeled and compared under pure current conditions. The two cages are reproductions of fish cages according to AKVA Group (2020): one is a circular cage, the other is a square cage. As shown in Fig. 2, the two cage models, corresponding to the illustrations in Fig. 1, have the same weight system as the multiple-sinker. The colored components refer to the floating collar (red), ropes (blue) and nettings (gray).

The nettings in the two fish cages have the same following parameters: solidity (Sn) of 0.25, twine diameter (d_w) of 1.5 mm and half mesh length (L) of 12 mm. The material properties of the nettings are assigned with Young's modulus (E) of 200 MPa and density of 1120 kg/m^3 to represent the Nylon material. The solidity in the present study indicates a realistic fish cage with little biofouling. For all cases, the netting has a cone-shaped bottom with a cone height of 3 m.

The ropes attached to the floating collar have a section diameter of 50 mm and are 1 m longer than the cage design height. The material of the rope is Polyethylene (PE) with Young's modulus (E) of 300 MPa and density of 1100 kg/m^3.

The sinkers are directly attached to the lowest end of the ropes. According to Cardia and Lovatelli (2015), the weight of sinkers is calculated mainly based on the expected current and is usually in a range of 40–70 kg/m in salmon farms. In the present study, the weight is 50 kg/m. Accordingly, the total weight of sinkers varies with the circumference of the cage, *i.e.*, for a fish cage with 120 m circumference, the total submerged weight of sinkers is $50 \times 120 = 6\ 000$ kg.

3. Numerical method

3.1. Structural model

3.1.1. Governing equations

In the present study, Code_Aster is used as the structural solver to calculate the structural responses of fish cages. The open-source Code_Aster, is developed by EDF R&D (Electricité de France (EDF), 1989), and is well verified according to Févotte and Lathuilière (2017).

The fish cage netting is divided into a set of line-type elements for calculating the structural responses. Based on the Cartesian coordinate system, the motions of Lagrangian nodes can be expressed with the differential equations as:

$$[\boldsymbol{M}]\ddot{\boldsymbol{q}} + [\boldsymbol{K}]\boldsymbol{q} = \boldsymbol{F}_g + \boldsymbol{F}_b + \boldsymbol{F}_h \tag{1}$$

where $\boldsymbol{q}$ is the time-dependent vector of nodal displacements, $\boldsymbol{M}$ is the mass matrix, $\boldsymbol{K}$ is the stiffness matrix, $\boldsymbol{F}_g$ is the nodal force vector due to gravity, $\boldsymbol{F}_b$ is the nodal force vector due to buoyancy, and $\boldsymbol{F}_h$ is the nodal force vector for the hydrodynamic forces. $\boldsymbol{F}_h$ is a time-dependent vector and calculated using the hydrodynamic model given in Section3.2. The other two force vectors, $\boldsymbol{F}_g$ and $\boldsymbol{F}_b$, are only calculated at the initialization step, which after, remain constant throughout the numerical simulation process. The system is highly nonlinear because of the last term ($\boldsymbol{F}_h$), on the right-hand side of Eq. (1), which is dependent on the

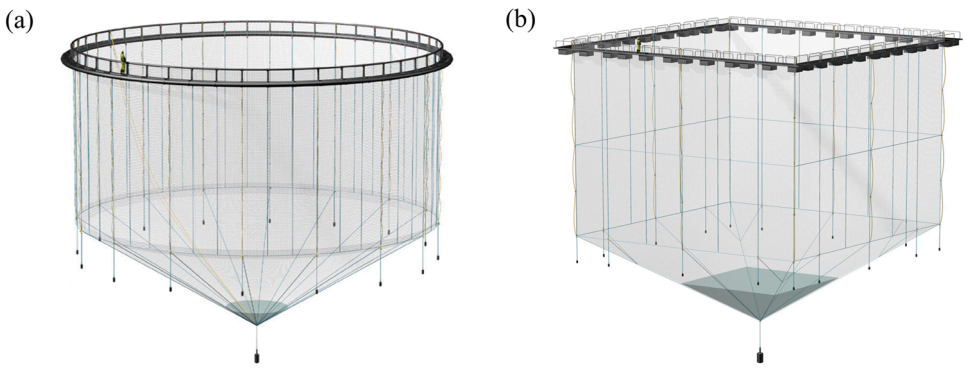

Fig. 1. Illustration of two fish cages: (a) is a circular fish cage and (b) is a square fish cage. These two cages employ the multiple-sinker weight system. The illustrations are gathered from a user manual by Egersund net (AKVA Group, 2020).

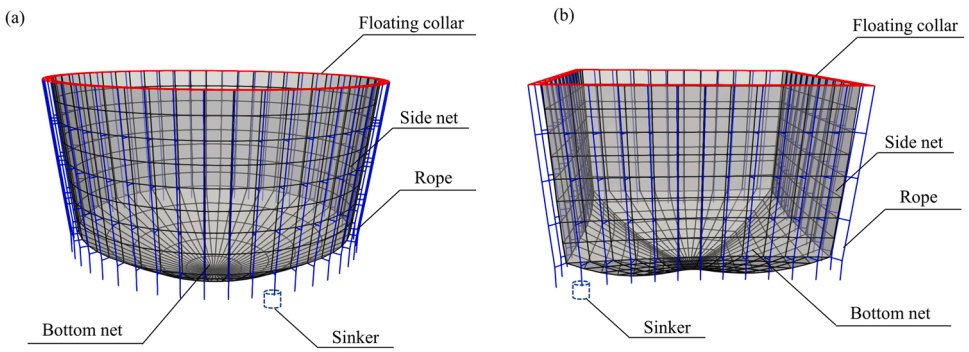

Fig. 2. Numerical models of the two fish cages. Note: Although only one sinker is shown in the illustrations, multiple sinkers are assembled at the lowest end of the ropes.

time, the square of nodal velocities, and the structural deformations.

According to Antonutti et al. (2018), the system nonlinearity can cause high-frequency oscillations and bring challenges for the simulations to convergence. These oscillations commonly occur in structural mechanics and are solved by introducing damping. In the present structural solver, Eq. (1) is solved by utilizing the unconditionally stable Hilber-Hughes-Taylor-α (HHT-α) method, proposed by Hilber et al. (1977). With a continuous variable timestep, the HHT-α method introduces low numerical damping in the low-frequency band and high damping at the high-frequency band (Antonutti et al., 2018). By implementing the HHT- α in Eq. (1), the discretized form in time can be expressed as:

$$\boldsymbol{M}\ddot{\boldsymbol{x}}_{i+1} + (1-\alpha)\boldsymbol{K}\boldsymbol{x}_{i+1} + \alpha\boldsymbol{K}\boldsymbol{x}_i = (1-\alpha)\left(\boldsymbol{F_g} + \boldsymbol{F_b} + \boldsymbol{F_h}\right)_{i+1} + \alpha\left(\boldsymbol{F_g} + \boldsymbol{F_b} + \boldsymbol{F_h}\right)_i \tag{2}$$

where the relation for the HHT- α is obtained together with the displacements and velocities in the following equations:

$$\boldsymbol{x}_{i+1} = \boldsymbol{x}_i + \Delta t\dot{\boldsymbol{x}}_i + \Delta t^2[(0.5-\beta)\ddot{\boldsymbol{x}}_i + \beta\ddot{\boldsymbol{x}}_{i+1}] \tag{3}$$

$$\dot{\boldsymbol{x}}_{i+1} = \dot{\boldsymbol{x}}_i + \Delta t[(1-\gamma)\ddot{\boldsymbol{x}}_i + \gamma\ddot{\boldsymbol{x}}_{i+1}] \tag{4}$$

where the parameters α, β and γ are satisfied:

$$0 \le \alpha \le \frac{1}{3}, \quad \beta = \frac{(1-\alpha)^2}{4}, \quad \gamma = \frac{1}{2} + \alpha \tag{5}$$

3.1.2. Finite element construction

The structural responses of fish cages mainly depend on the nettings, ropes and bottom weights. The structural element used in the present study is a one-dimensional finite element denoted as "CABLE" in the structural solver, which was initially developed to calculate the mechanical behavior of overhead electrical lines. This element is a version of the classic two-node "bar" element but can only bear tensions. It is suitable for representing highly flexible line-like structures (Antonutti et al., 2018), and thus, suitable for modeling of the nettings and ropes. The weights at the lowest end of ropes are modeled as constant forces, ignoring their shapes and hydrodynamic loads.

3.2. Hydrodynamic model

3.2.1. Hydrodynamic model for netting

Based on a large number of experiments (Balash et al., 2009; Lader et al., 2014; Tang et al., 2018; Tsukrov et al., 2011), researchers found that the hydrodynamic characteristics of for nettings are mainly dependent on the two dimensionless variables, *Sn* and *Re*. For square-mesh nettings, the first dimensionless variable, *Sn*, can be expressed as:

$$Sn = \frac{2d_w}{L} - \left(\frac{d_w}{L}\right)^2 \tag{6}$$

where d_w is the twine diameter and L is the half mesh size, as illustrated in Fig. 3. The solidity ratio for aquaculture netting is in the range of 0.19–0.43, including biofouling (Kristiansen and Faltinsen, 2012).

The second dimensionless variable, *Re*, is defined as:

$$Re = \frac{Ud_w}{\nu} \tag{7}$$

where U is the undisturbed fluid velocity, d_w is the twine diameter and ν is the kinematic viscosity of the fluid. The typical Reynolds number for fish cage nettings is in the range of 100–10 000 (Cheng et al., 2020).

In the present study, hydrodynamic forces on nettings are calculated based on Screen models. According to Cheng et al. (2020), Screen models are theoretically superior to Morison models, because the twine-to-twine interaction is implicitly included in the force calculation. Fig. 4 illustrates the screen model that is used in the present study to calculate the hydrodynamic forces ($\boldsymbol{F_h}$) on the netting. The hydrodynamic forces are decomposed into drag force $\boldsymbol{F_D}$ Eq. (8) and lift force $\boldsymbol{F_L}$ Eq. (9):

$$\boldsymbol{F_D} = \frac{1}{2}C_D\rho_w A_t|\boldsymbol{U_c} - \boldsymbol{v}|^2\boldsymbol{i_D} \tag{8}$$

$$\boldsymbol{F_L} = \frac{1}{2}C_L\rho_w A_t|\boldsymbol{U_c} - \boldsymbol{v}|^2\boldsymbol{i_L} \tag{9}$$

where ρ_w is the fluid density, A_t is the area of the net panel, $\boldsymbol{U_c}$ is the velocity of the fluid at the centroid of the net panel and $\boldsymbol{v}$ is the velocity of the structure. C_D and C_L are the drag and lift force coefficients in Screen model, respectively. The unit vectors $\boldsymbol{i_D}$ and $\boldsymbol{i_L}$ which are used to indicate the directions of drag and lift force and are defined by Eqs. (10) - (12).

$$\boldsymbol{i_D} = \frac{\boldsymbol{U_c} - \boldsymbol{v}}{|\boldsymbol{U_c} - \boldsymbol{v}|} \tag{10}$$

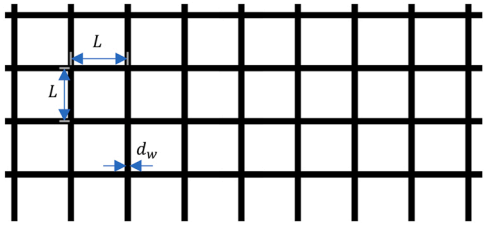

Fig. 3. Illustration of the twine diameter d_w and half mesh size L for a square-mesh netting.

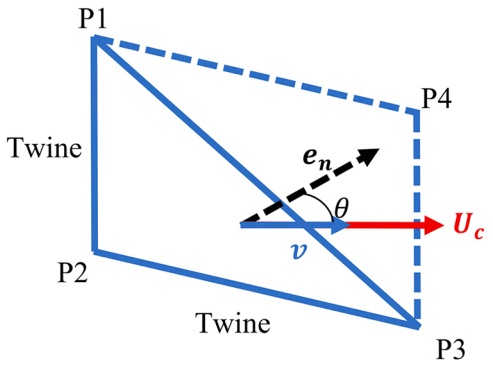

Fig. 4. Illustration of a net panel in Screen model. The inflow angle θ of the net panel is the angle between the normal vector $\boldsymbol{e_n}$ and current velocity $\boldsymbol{U_c}$.

$$\boldsymbol{i_L} = \frac{(\boldsymbol{U_c} - \boldsymbol{v}) \times \boldsymbol{e_n} \times (\boldsymbol{U_c} - \boldsymbol{v})}{|(\boldsymbol{U_c} - \boldsymbol{v}) \times \boldsymbol{e_n} \times (\boldsymbol{U_c} - \boldsymbol{v})|} \tag{11}$$

$$\boldsymbol{e_n} = \frac{\overrightarrow{P1P2} \times \overrightarrow{P1P3}}{\left|\overrightarrow{P1P2} \times \overrightarrow{P1P3}\right|} \tag{12}$$

The force coefficients employed in this study are originally proposed by (Kristiansen and Faltinsen, 2012), and are expressed as Eqs. (13)-(20). The drag and lift coefficients are expressed respectively as:

$$C_D = C_{D0}(0.9cos\theta + 0.1cos3\theta) \tag{13}$$

$$C_L = C_{L0}(sin2\theta + 0.1sin4\theta) \tag{14}$$

$$C_{D0} = C_{cylinder}\frac{Sn(2 - Sn)}{2(1 - Sn)^2} \tag{15}$$

$$C_{L0} = \frac{0.5C_{D0} - C_{L45}}{\sqrt{2}} \tag{16}$$

$$C_{L45} = \frac{\pi C_{N45}}{8 + C_{N45}} \tag{17}$$

$$C_{N45} = C_{cylinder}\frac{Sn}{2(1 - Sn)^2} \tag{18}$$

$$\begin{aligned} C_{cylinder} = & -78.46675 + 254.73873(log_{10}Re) - 327.8864(log_{10}Re)^2 \\ & + 223.64577(log_{10}Re)^3 - 87.92234(log_{10}Re)^4 + 20.00769(log_{10}Re)^5 \\ & - 2.44894(log_{10}Re)^6 \quad + 0.12479(log_{10}Re)^7 \end{aligned} \tag{19}$$

$$Re = \frac{d_{w0}(\boldsymbol{U_c} - \boldsymbol{v})}{\nu(1 - Sn)}, \quad 10^{3/2} \le Re \le 10^4 \tag{20}$$

3.2.2. Hydrodynamic model for floating collar and cables

For the ropes and the HDPE floating collar, the hydrodynamic forces are calculated based on the Morison model (Morison et al., 1950). The hydrodynamic forces are decomposed into the two components, *i.e.*, normal drag force ($\boldsymbol{F_n}$, Eq. (21)) and tangential drag force ($\boldsymbol{F_t}$, Eq. (22)), which are expressed as:

$$\boldsymbol{F_n} = \frac{1}{2}C_n\rho L d_w|\boldsymbol{u^r}_n|\boldsymbol{u^r}_n \tag{21}$$

$$\boldsymbol{F_t} = \frac{1}{2}C_t\rho L d_w|\boldsymbol{u^r}_t|\boldsymbol{u^r}_t \tag{22}$$

where L is the length of ropes or HDPE pipes, d_w is the section diameter, ρ is the fluid density. $\boldsymbol{u^r}_n$ and $\boldsymbol{u^r}_t$ are the normal and tangential velocity of fluid relative to the twine. C_n and C_t are the normal and tangential drag coefficients. The two force coefficients employed in this study originates from DeCew et al. (2010) and are expressed by Eqs. (23)-(26). A 2D illustration of the force decomposition is given in Fig. 5.

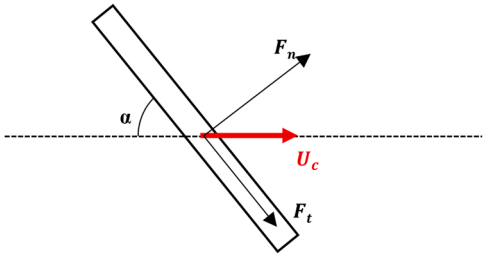

Fig. 5. A 2D illustration of the hydrodynamic forces on cables or pipes. $\boldsymbol{F_n}$ and $\boldsymbol{F_t}$ are the normal and tangential drag forces, respectively. The angle of attack α is the angle between the current direction and the axis of the cable or pipes.

$$C_n = \begin{cases} \dfrac{8\pi}{sRe}\left(1 - 0.87s^{-2}\right) & 0 < Re < 1 \\ 1.45 + 8.55Re^{-0.9} & 1 < Re < 30 \\ 1.1 + 4Re^{-0.5} & 30 < Re < 2.33 \times 10^5 \\ -3.41 \times 10^{-6}\left(Re - 5.78 \times 10^5\right) & 2.33 \times 10^5 < Re < 4.92 \times 10^5 \\ 0.401\left(1 - e^{-\frac{Re}{5.99} \times 10^5}\right) & 4.92 \times 10^5 < Re < 10^7 \end{cases} \tag{23}$$

$$C_t = \pi\mu\left(0.55\sqrt{Re} + 0.084Re^{\frac{2}{3}}\right) \tag{24}$$

$$s = -0.077215665 + ln(8/Re); \tag{25}$$

$$Re = \frac{d_w(u_n - v_n)}{\nu} \tag{26}$$

3.3. Wake effect

When the current passes through a net panel, the current velocity will be reduced by the friction from the twines in the net panel. This velocity-reduced current results in a smaller drag force on downstream net panels compared to upstream ones. In order to accurately predict the drag forces, it is necessary to know how much the velocity is reduced in the wake. In practice, a flow reduction factor (r) is adopted to address this current velocity reduction, as expressed by $\boldsymbol{U}_{downstream} = r\boldsymbol{U}_\infty$ ($0 < r < 1$), where $\boldsymbol{U}_{downstream}$ is the current velocity in the wake and $\boldsymbol{U}_\infty$ is incoming velocity. In this study, the flow reduction factor is from the velocity profiles based on high-fidelity numerical simulations by Cheng et al. (2022).

3.4. Simulation process

The studied parameters in the present study are given in Table 1. The dimensions of the fish cage include circumference (C) and design height (H). The current velocity (U) is assumed uniform within the water depth.

In order to study the effects of design parameters on the cultivation volumes and drag forces, 5 circumferences, 5 design heights and 7 current velocities are considered in the investigation. Together with the

Table 1
Summary of simulation cases.

Parameter	Variable	Value	Unit
Circumference	C	100,120, 140, 160, 180	m
Design height	H	10, 20, 30, 40, 50	m
Current velocity	U	0, 0.1, 0.2, 0.3, 0.4, 0.5, 0.6	m/s

two types of fish cages, there are $5 \times 5 \times 7 \times 2 = 350$ simulation cases in total. The simulation process is presented in Fig. 6, where an external module is invoked at each time step to calculate the hydrodynamic forces on the nets, cables and HDPE pipes and maps the forces onto corresponding nodes in the structural elements. Two types of hydrodynamic models, *i.e.* Screen model and Morison model, are applied to nettings and cables, respectively. In order to compare the stable results, the fish cages are exposed to a pure current velocity for 60 s with a time step of 0.1 s. The mean value of the drag force and cultivation volume is measured from the last 10 s of the simulation process when the fish cages reach a stable condition.

3.5. Key parameters for measurement

Currently, there are several approaches to estimate the volume of fish cages, including the scalar triple product method, divergence theorem method and the stack of pies method (Xu and Qin, 2020). Overall, these approaches can provide equivalent results given the same discretization level. In this study, the fish cage volume is calculated using the scalar triple product method. The cultivation volume is calculated as:

$$V = \sum_{i=1}^{N} \frac{1}{6} |P1 \bullet (P2 \times P3)| \tag{27}$$

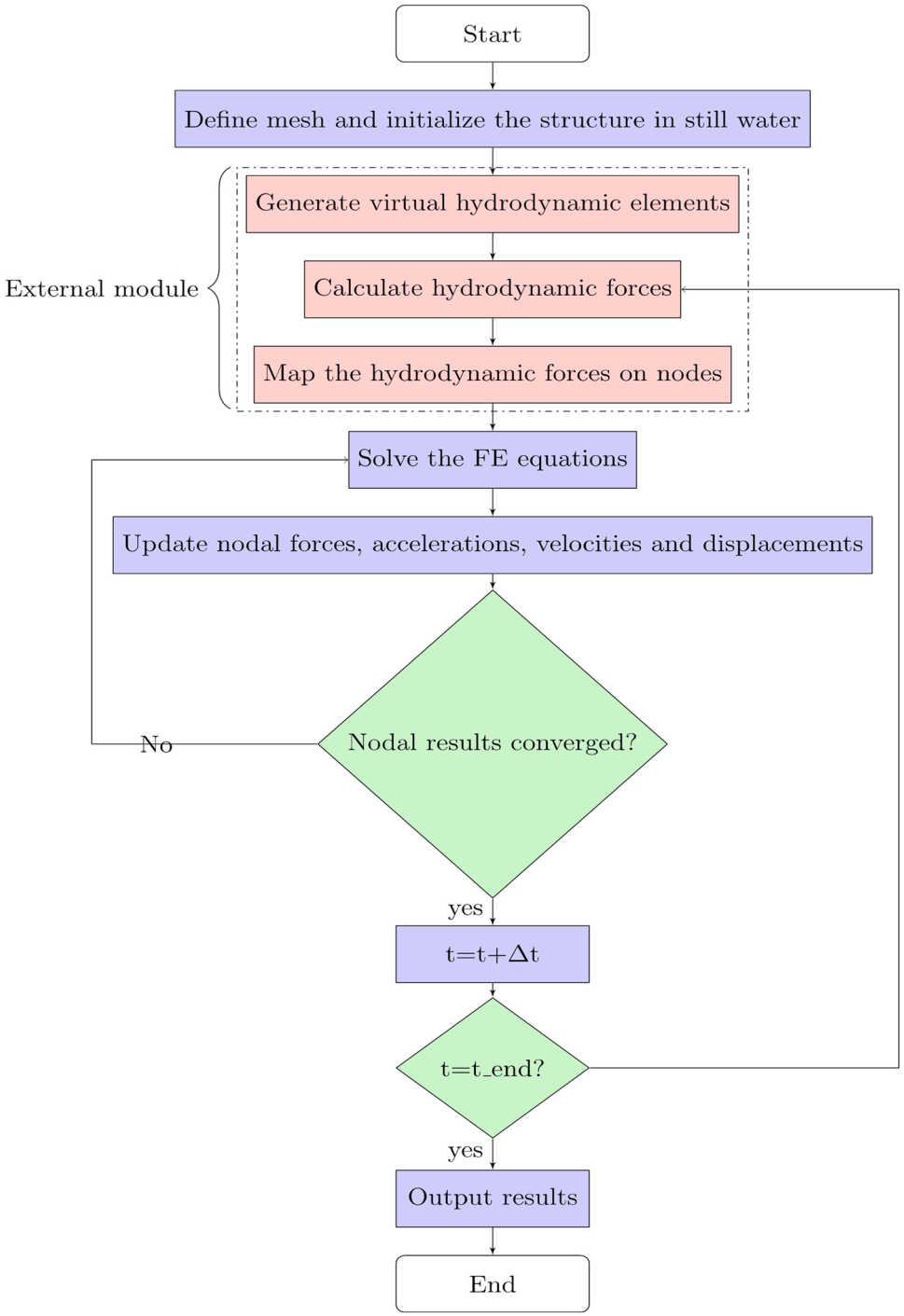

Fig. 6. Reproduction of the simulation process for the numerical solver originally proposed by Cheng et al. (2020).

where cultivation volume is represented as V, N is the number of net panel elements to embrace the cage. $P1$, $P2$ and P3 are the coordinates of the vertices in a net panel, as shown in Fig. 2.

The volume reduction factor Vr is defined as a fraction between the volume when the fish cage is subjected to the velocity and the initial fish cage volume in still water, and it is expressed as:

$$V_r = \frac{V}{V_0} \tag{28}$$

where V is the mean cultivation volume based on the last 10 s simulation results and V_0 is the initial volume in the still water ($U = 0$ m/s).

4. Results and discussion

4.1. Cage deformation

Fig. 7 shows the deformation of the two cages under different current velocities. When the fish cages are exposed to current velocities, the netting can have observable deformations. As observed from Fig. 7. both cages have the same following deformation characteristics: (1) the nettings drift horizontally along the current direction, (2) the draft of the cage is reduced as the bottom net is lifted, and (3) the side net narrow towards the center of the cage. However, the two cages have distinctive deformation on the bottom nets. The square cage has a cruciform pattern on the bottom nets, and this pattern becomes obvious when $U > 0.3$ m/s. However, the circular cage does not have this cruciform pattern. A possible explanation for the cruciform pattern only appearing in the square cage might be that current-induced drag forces on the front- and back-side nets are much larger than those on the two side nets which are parallel to the current direction. With the constant weight per meter at the bottom sinkers, the front- and back-side nets will have larger horizontal drifts than the two side nets. Thus, the cruciform pattern can be seen on the bottom nets of square cages.

Fig. 8 illustrates the deformations of the two cages with varying circumferences from the side view. The deformed cages with different circumferences almost have a similar degree of obliquity. This similar degree of obliquity implies that the increased current loads due to the larger circumference may be compensated by the increased total weight. With this hypothesis, the current load on the fish cage should increase linearly with the circumference, as the total weight is increased linearly with the circumference. The later discussion in Section 4.3 provides evidence to prove this hypothesis.

Fig. 9 illustrates the deformations of the two cages with varying design heights from the side view. As shown in Fig. 9, the cage with larger design heights has a larger horizontal drift. As the current load on the fish cage is increased with the increasing design height, the constant total weights cannot compensate for the increased current load. Thus, the cage with a smaller design height may have a smaller degree of

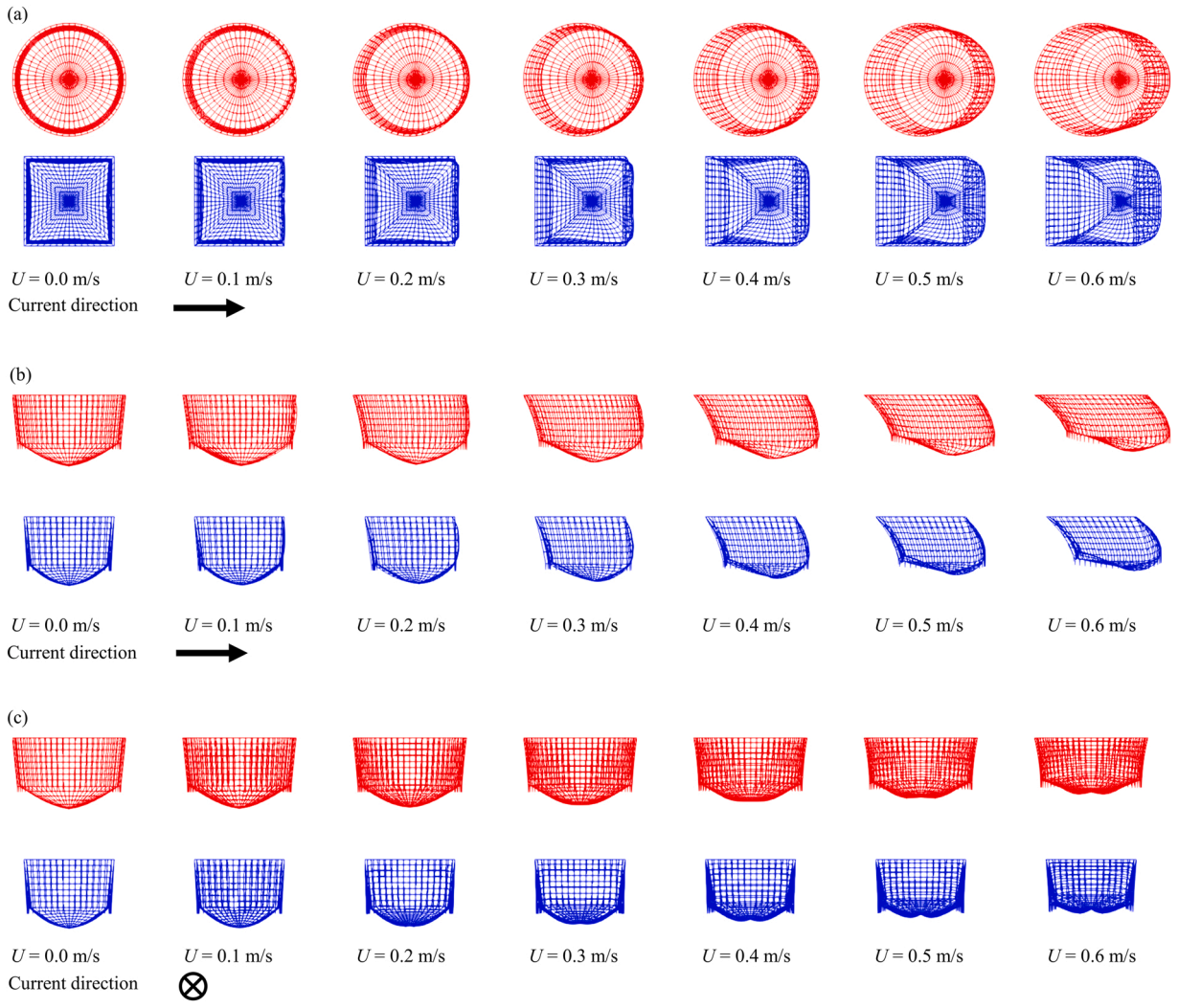

Fig. 7. Deformations of fish cages with respect to different current velocities where the circular (red) and square (blue) cages are shown from top (a), side (b) and front (c). Both fish cage have $C = 140$ m and $H = 20$ m.

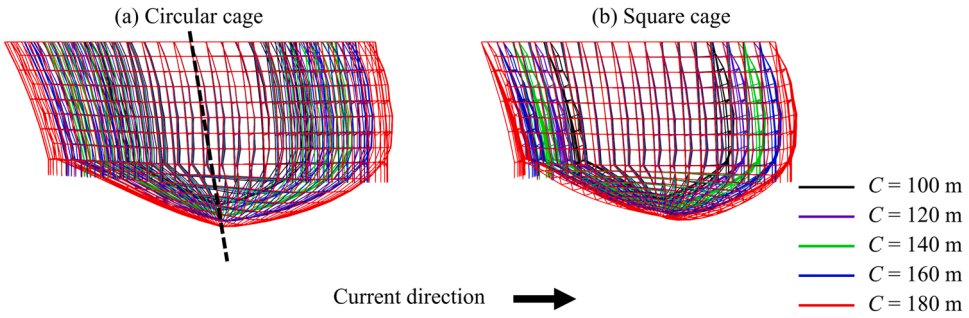

Fig. 8. Deformations of the two cages with varying conferences when $H = 20$ m and $U = 0.3$ m/s.

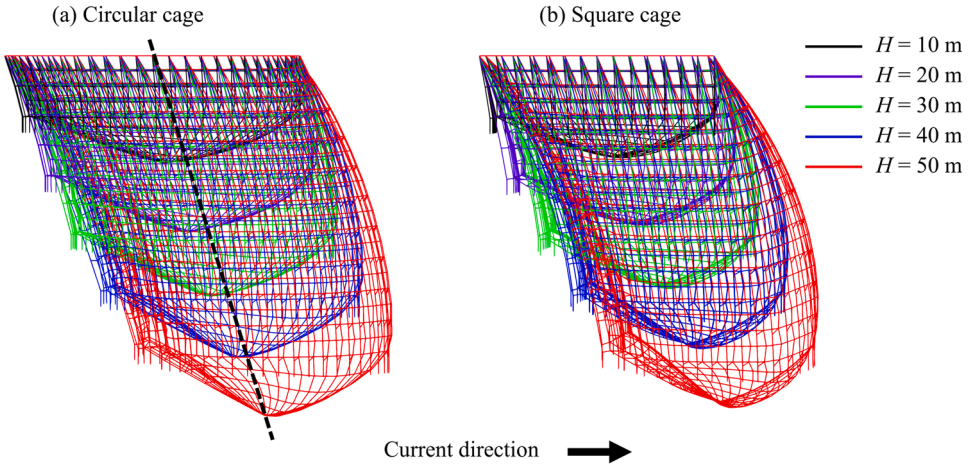

Fig. 9. Deformations of the two cages with varying design heights when $C = 140$ m and $U = 0.3$ m/s.

obliquity. Based on this observation, the design height of a cage should not be too large in order to avoid the unwanted horizontal drift.

4.2. Cultivation volume

Because the netting is flexible, the cultivation volume decreases with the increasing current velocity. The decreased cultivation volume due to large current loads can shrink the living space for the cultured fish and pose a negative impact on fish welfare. Consequently, it is critical to assess the volume reduction due to the environmental impacts at the fish farming site. As shown in Fig. 10, the cultivation volumes of both cages decrease with the increasing current velocity. Within the same circumference, design height and current velocity, the circular cage has a larger cultivation volume than the square cage.

Fig. 10 also that the cultivation volume increases significantly with the increasing circumferences. In addition, the cage with a smaller circumference has a smaller volume reduction with the increasing current velocity. This implies that the cage with a smaller circumference may be more suitable for exposed sites due to its smaller volume reduction under strong current.

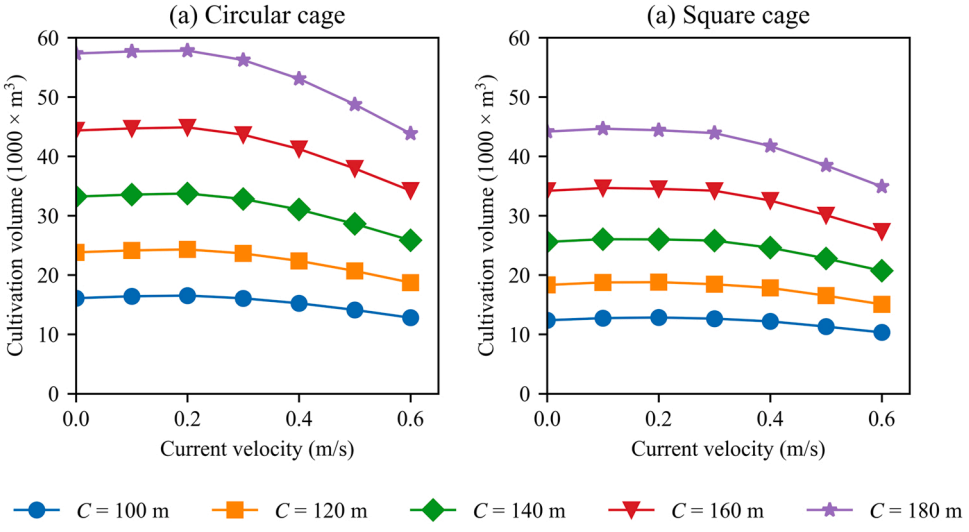

Fig. 10. Cultivation volume of the two cages under different current velocities when $H = 20$ m.

Fig. 11 shows the cultivation volume of the two cages with the same circumference but varying design heights under different current velocities. The circular cage has a larger cultivation volume when the two cages have the same circumference, design height and under the same current velocity. Cage with larger design height can gain larger cultivation volume. However, the current load can significantly reduce the cultivation volume. In addition, the benefit of increasing design heights is promising only when the current velocity is small (*i.e.*, < 0.3 m/s). Thus, increasing the design height of this gravity-type cage can only bring limited cultivation volume to a cage at exposed sites.

The cost of nettings accounts for a large amount of the total cost of the cage construction. In order to obtain a large cultivation volume for the fish, the dimension of the cage usually has to increase. Increasing the cage dimension can significantly increase the initial cost of a fish farm. Fig. 12 shows the cultivation volume of the two cages with different dimensions in still water and under a current of 0.6 m/s. As discussed in the previous sections and also shown in Fig. 12, circular cages can gain a larger cultivation volume than the square cages with the same circumference, design height and under the same current velocity. The relationship between the netting area and cultivation volume is described using Eq. (29) whose coefficients are given in Table 2. The relationships indicate that the circular cage is more economical than the square cage, as the circular cage has a larger cultivation volume per netting area than the square cage under the same current velocity. Especially for the large cage (*i.e.*, the cultivation volume is larger than 100,000 m^3), the economic benefit of the circular cage is more noticeable. For example, a 100,000 m^3 circular cage can save approximately 15% netting than a square cage with the same volume. However, the economic advantage of the circular cage is insignificant when the cage is small. When the cultivation volume is less than 20,000 m^3, these two types of cage need approximately the same area of nettings.

$$V = \quad aA^{1.5} + b \tag{29}$$

4.3. Volume reduction factor

Fig. 13 shows the volume reduction factor of the two fish cages with respect to current velocities, design heights and circumferences. In general, the square cage has a larger volume reduction factor than the circular cage, especially for the cages with small circumference and large design height. Strong current can reduce the cultivation volume significantly, but when the current velocity is smaller than 0.2 m/s, the cultivation volume of the cage is almost the same as in still water. With the constant weight per meter at the bottom sinkers, increasing the circumferences has an unnoticeable influence on the volume reduction factor, while increasing the design height can significantly reduce the volume reduction factor. Thus, the optimal way to increase the cultivation volume of a cage is to increase its circumference.

4.4. Drag force

Fig. 14 shows the drag force on the two fish cages with respect to current velocities. In general, the drag force on fish cages increases nonlinearly with the increasing velocity. Additionally, the circular cage experiences a larger drag force than the square cage with the same circumference, design height and current velocity.

As shown in Fig. 15, increasing the circumference of a fish cage can obviously bring additional drag force. Moreover, the drag forces on both cages linearly increase with the increasing circumferences under a given velocity. This linear-increasing drag force together with the linear-increasing total weight for the cage with varying circumference causes the similar cage deformation that is discussed in Section 4.1.

Fig. 16 shows the drag force on the two fish cages with varying design heights. Overall, an increase of the design height results in larger drag forces on both fish cages. Different from the increasing circumference, the drag force is not linearly increased with the increasing design height, especially when $U > 0.4$ m/s.

Fig. 17 shows the relationship between drag force and cultivation volume for the cages with different dimensions. For a given current velocity, the larger cage experiences a larger drag force. Moreover, a cage with a larger cultivation volume in still water can have a larger volume variation under a strong current. The dashed lines in Fig. 17 indicate that with the increasing current velocity, the cultivation volume is reduced, and the drag force is increased at the same time. In addition, the scatter plots also indicate that the square cage has a larger drag force per cultivation volume than the circular fish cage.

Fig. 18 shows the relationship between the normalized drag force and the volume reduction factor. The normalized drag force is defined as the ratio of the drag force and total bottom weight. The experimental results from Dong et al. (2021), where the drag forces and cage deformations of a scaled circular cage model are investigated in detail, are also shown in Fig. 18 for comparison. As shown in Fig. 18(a), the numerical results in the present study agree well with the experiments by Dong et al. (2021), especially when $U > 0.4$ m/s. This good agreement can validate the results of the present simulation. The discrepancy between the numerical and experimental results under small current velocity may come from that the scaled current speed in that experiments can only reflect the strong currents in the full-scale circumstances. In

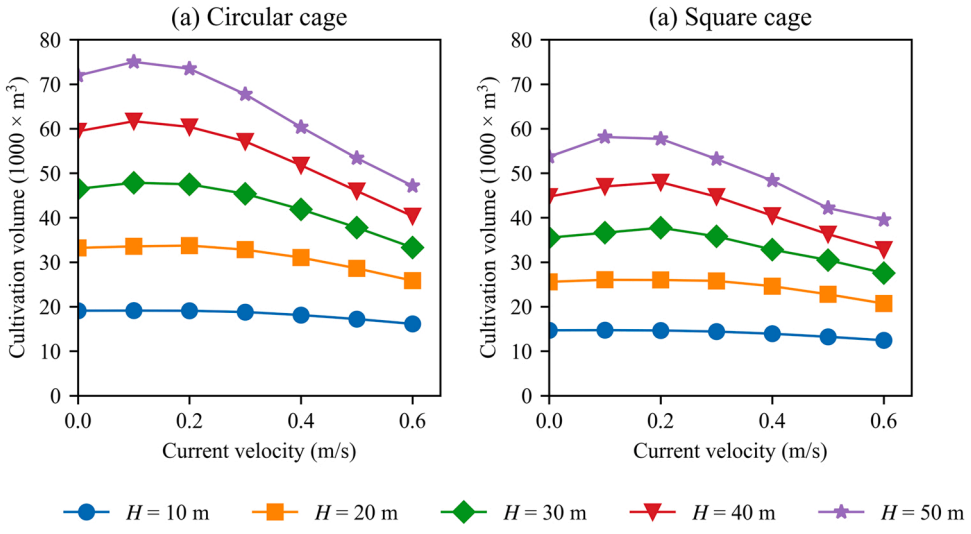

Fig. 11. Cultivation volume of the two cages under different current velocities when $C = 140$ m.

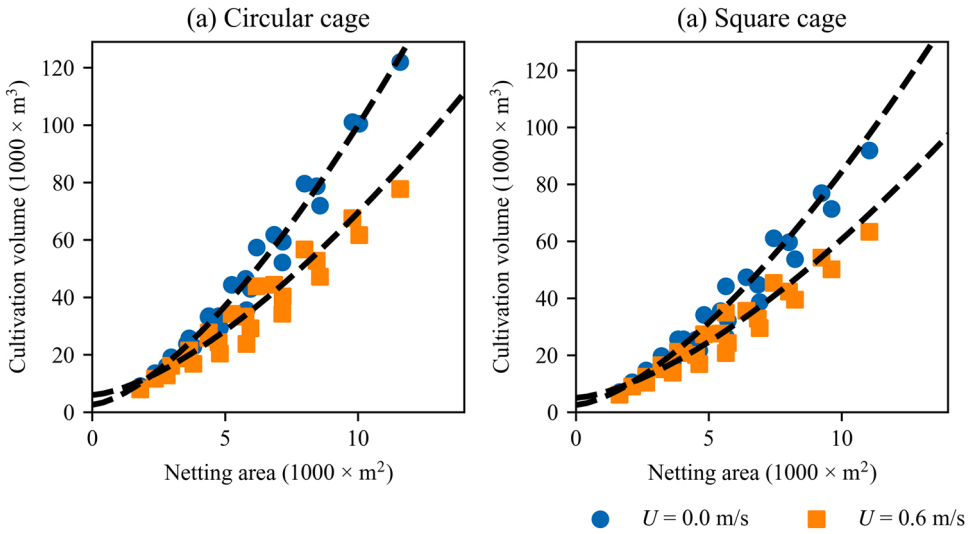

Fig. 12. Cultivation volume of the two cages with different dimensions. The dashed lines in each subplot are the regression curves based on Eq. (29).

Table 2
Regression coefficients for Eq. (29).

Cage shape	$U = 0.0$ m/s			$U = 0.6$ m/s		
	a	b	R^2	a	b	R^2
Circular cage	3.08	2.54	0.977	2.01	5.95	0.942
Square cage	2.99	2.49	0.952	1.76	5.0	0.932

addition, given the same normalized drag force, the square cage can have a larger volume reduction factor than the circular cage.

5. Conclusion

In this study, the structural responses of two typical gravity-based fish cages with circular and square shapes are analysed with different dimensions and current velocities. The following conclusions are drawn from this study:

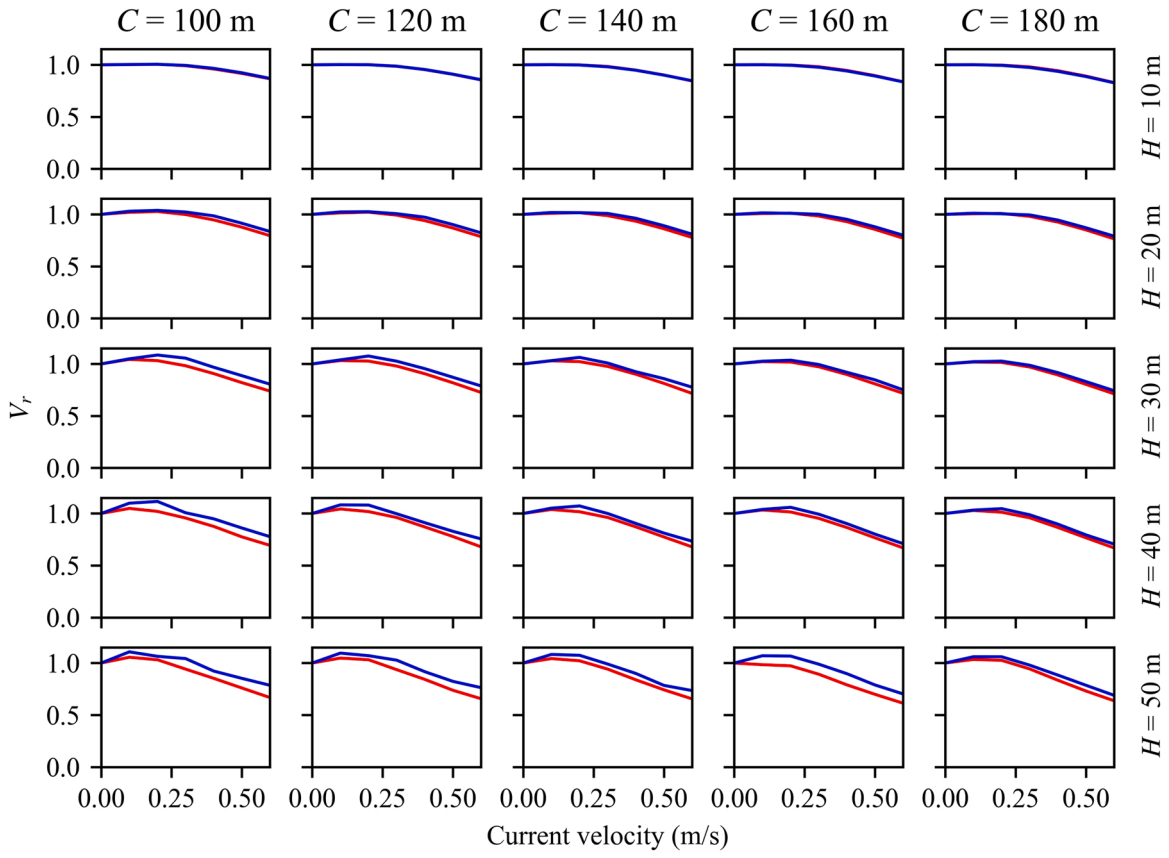

Fig. 13. Volume reduction factor of the two fish cages with respect to different current velocities, design heights and circumferences. The red and blue lines refer to the circular and the square cage, respectively.

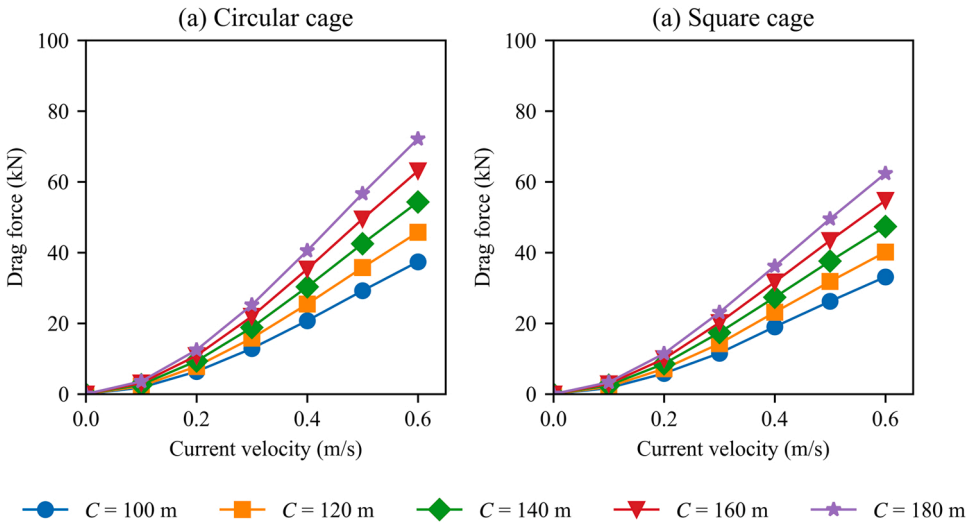

Fig. 14. Drag force on the two fish cages under different current velocities when $H = 20$ m.

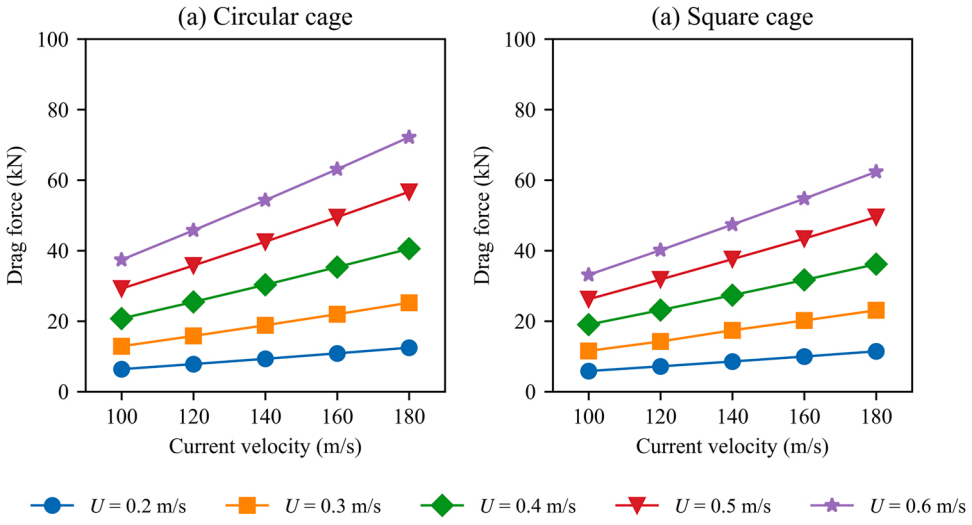

Fig. 15. Drag force of the cages with varying circumferences when $H = 20$ m.

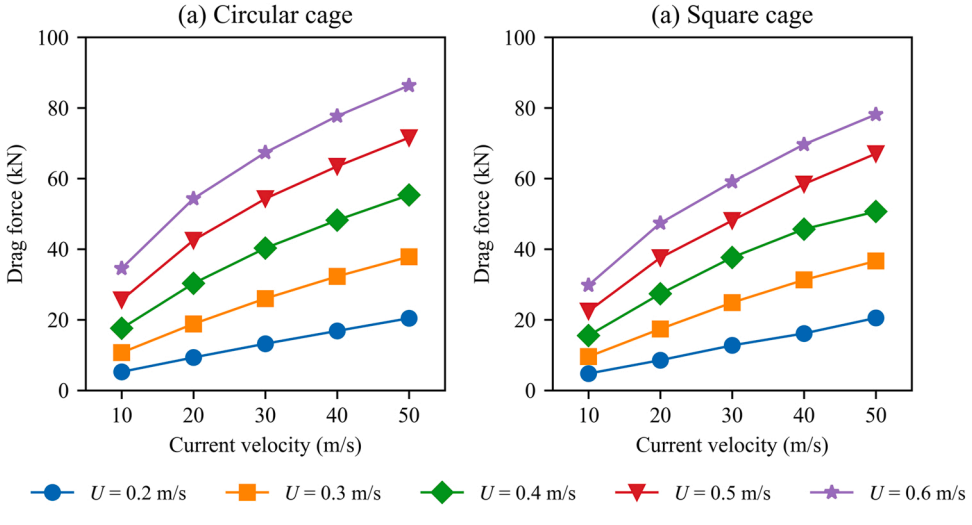

Fig. 16. Drag force on the two fish cages with varying design heights when $C = 140$ m.

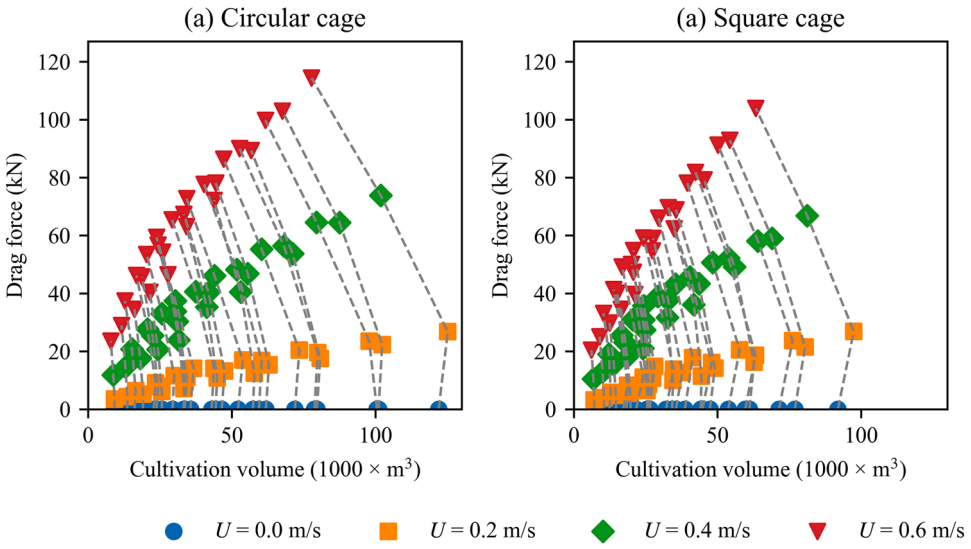

Fig. 17. Relationship between drag force and cultivation volume.

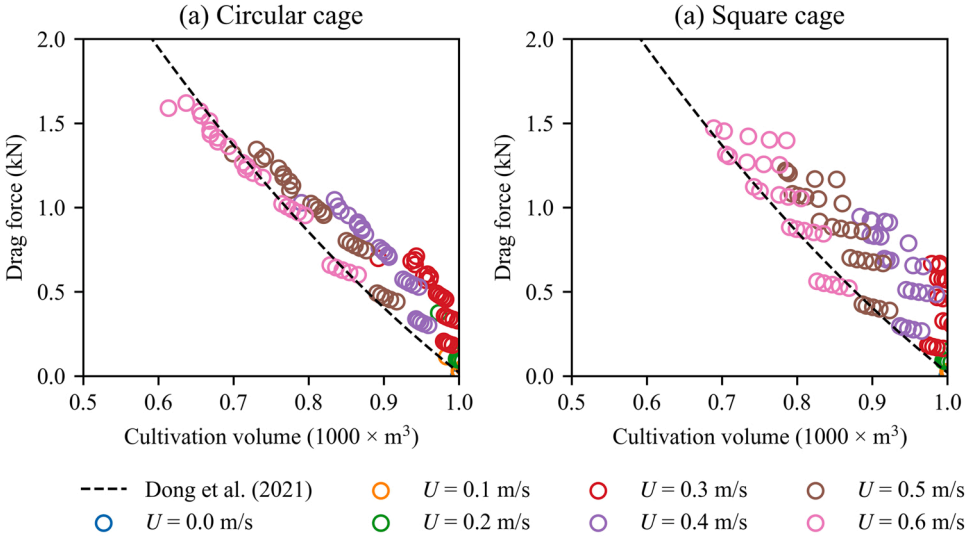

Fig. 18. Relationship between normalized drag forces and volume reduction factor.

- Given the same circumference, design height and current velocity, the square fish cage has a smaller cultivation volume than the circular cage.
- From the economic point of view, the circular cage can gain more cultivation volume than the square cage given the same area of netting. However, this economic advantage of the circular cage is insignificant when the cage volume is less than 20,000 m^3.
- Increasing circumference is more efficient than increasing design height for the improvement of cultivation volume.
- With the constant weight per meter, the drag force on both fish cages increases non-linearly with the increasing current velocity and the increasing design height, but almost linearly with the increasing circumference.
- The circular fish cage has less drag force per cultivation volume than the square fish cage.

CRediT authorship contribution statement

Magnus Aske Mjåtveit: Conceptualization, Methodology, Validation, Formal analysis, Investigation, Writing – original draft, Writing – review & editing, Visualization. **Hui Cheng**: Conceptualization, Methodology, Software, Validation, Formal analysis, Investigation, Writing – original draft, Writing – review & editing, Visualization, Supervision, **Muk Chen Ong**: Conceptualization, Resources, Investigation, Writing – review & editing, Supervision, Project administration, Funding acquisition, **Jihoon Lee**: Conceptualization, Investigation, Writing – review & editing.

Declaration of Competing Interest

The authors declare that they have no known competing financial interests or personal relationships that could have appeared to influence the work reported in this paper.

References

AKVA Group, 2020. Pen Farming Aquaculture Catalogue (English).
Antonutti, R., Peyrard, C., Incecik, A., Ingram, D., Johanning, L., 2018. Dynamic mooring simulation with Code_Aster with application to a floating wind turbine. Ocean Eng. 151, 366–377. https://doi.org/10.1016/j.oceaneng.2017.11.018.

Balash, C., Colbourne, B., Bose, N., Raman-Nair, W., 2009. Aquaculture net drag force and added mass. Aquac. Eng. 41, 14–21. https://doi.org/10.1016/j.aquaeng.2009.04.003.

Brizzi, G., Sabbagh, M., 2021. A new criterion for multi-purpose platforms siting: fish endurance to wave motion within offshore farming cages. Ocean Eng. 224, 108751 https://doi.org/10.1016/j.oceaneng.2021.108751.

Cardia, F., Lovatelli, A., 2015. Aquaculture Operations in Floating HDPE Cages: A Field Handbook. Food and Agriculture Organization of the United States,, Rome.

Chen, D., Wang, C.M., Zhang, H., 2021. Examination of net volume reduction of gravity-type open-net fish cages under sea currents. Aquac. Eng. 92, 102128 https://doi.org/10.1016/j.aquaeng.2020.102128.

Cheng, H., Li, L., Aarsæther, K.G., Ong, M.C., 2020. Typical hydrodynamic models for aquaculture nets: a comparative study under pure current conditions. Aquac. Eng. 90, 102070 https://doi.org/10.1016/j.aquaeng.2020.102070.

Cheng, H., Ong, M.C., Li, L., Chen, H., 2022. Development of a coupling algorithm for fluid-structure interaction analysis of submerged aquaculture nets. Ocean Eng. 243, 110208 https://doi.org/10.1016/j.oceaneng.2021.110208.

DeCew, J., Tsukrov, I., Risso, A., Swift, M.R., Celikkol, B., 2010. Modeling of dynamic behavior of a single-point moored submersible fish cage under currents. Aquac. Eng. 43, 38–45. https://doi.org/10.1016/j.aquaeng.2010.05.002.

Dong, S., You, X., Hu, F., 2021. Experimental investigation on the fluid–structure interaction of a flexible net cage used to farm Pacific bluefin tuna (Thunnus orientalis). Ocean Eng. 226, 108872 https://doi.org/10.1016/j.oceaneng.2021.108872.

Electricité de France (EDF), 1989. Finite Element Code_Aster, Analysis of Structures and Thermomechanics for Studies and Research.

Endresen, P.C., Klebert, P., 2020. Loads and response on flexible conical and cylindrical fish cages: a numerical and experimental study based on full-scale values. Ocean Eng. 216, 107672 https://doi.org/10.1016/j.oceaneng.2020.107672.

Food and Agriculture Organization, 2020. The State of World Fisheries and Aquaculture 2020: Sustainability in Action, The State of World Fisheries and Aquaculture (SOFIA). FAO,, Rome, Italy.

Hilber, H.M., Hughes, T.J.R., Taylor, R.L., 1977. Improved numerical dissipation for time integration algorithms in structural dynamics. Earthq. Eng. Struct. Dyn. 5, 283–292. https://doi.org/10.1002/eqe.4290050306.

Huang, C.-C., Tang, H.-J., Liu, J.-Y., 2006. Dynamical analysis of net cage structures for marine aquaculture: numerical simulation and model testing. Aquac. Eng. 35, 258–270. https://doi.org/10.1016/j.aquaeng.2006.03.003.

Huang, C.-C., Tang, H.-J., Liu, J.-Y., 2007. Modeling volume deformation in gravity-type cages with distributed bottom weights or a rigid tube-sinker. Aquac. Eng. 37, 144–157. https://doi.org/10.1016/j.aquaeng.2007.04.003.

Hvas, M., Folkedal, O., Oppedal, F., 2021. Fish welfare in offshore salmon aquaculture. Rev. Aquacult. 13, 836–852. https://doi.org/10.1111/raq.12501.

Jin, J., Su, B., Dou, R., Luan, C., Li, L., Nygaard, I., Fonseca, N., Gao, Z., 2021. Numerical modelling of hydrodynamic responses of Ocean Farm 1 in waves and current and validation against model test measurements. Mar. Struct. 78, 103017 https://doi.org/10.1016/j.marstruc.2021.103017.

Jónsdóttir, K.E., Hvas, M., Alfredsen, J.A., Føre, M., Alver, M.O., Bjelland, H.V., Oppedal, F., 2019. Fish welfare based classification method of ocean current speeds at aquaculture sites. Aquac. Environ. Interact. 11, 249–261. https://doi.org/10.3354/aei00310.

Kristiansen, T., Faltinsen, O.M., 2012. Modelling of current loads on aquaculture net cages. J. Fluids Struct. 34, 218–235. https://doi.org/10.1016/j.jfluidstructs.2012.04.001.

Lader, P., Enerhaug, B., Fredheim, A., Klebert, P., Pettersen, B., 2014. Forces on a cruciform/sphere structure in uniform current. Ocean Eng. 82, 180–190. https://doi.org/10.1016/j.oceaneng.2014.03.007.

Lee, C.-W., Kim, Y.-B., Lee, G.-H., Choe, M.-Y., Lee, M.-K., Koo, K.-Y., 2008. Dynamic simulation of a fish cage system subjected to currents and waves. Ocean Eng. 35, 1521–1532. https://doi.org/10.1016/j.oceaneng.2008.06.009.

Li, L., Jiang, Z., Ong, M.C., Hu, W., 2019. Design optimization of mooring system: an application to a vessel-shaped offshore fish farm. Eng. Struct. 197, 109363 https://doi.org/10.1016/j.engstruct.2019.109363.

Li, Y., Zhao, Y., Gui, F., Teng, B., Guan, C., 2006. Numerical analysis of the effects of sinker weight on the hydrodynamics behaviour of gravity cage net in uniform flow. J. Hydrodyn. Ser. B 18, 77–83. https://doi.org/10.1016/S1001-6058(06)60034-6.

Moe-Føre, H., Lader, P.F., Lien, E., Hopperstad, O.S., 2016. Structural response of high solidity net cage models in uniform flow. J. Fluids Struct. 65, 180–195. https://doi.org/10.1016/j.jfluidstructs.2016.05.013.

Morison, J.R., Johnson, J.W., Schaaf, S.A., 1950. The force exerted by surface waves on piles. J. Pet. Technol. 2, 149–154. https://doi.org/10.2118/950149-G.

Ruzzo, C., Muggiasca, S., Malara, G., Taruffi, F., Belloli, M., Collu, M., Li, L., Brizzi, G., Arena, F., 2021. Scaling strategies for multi-purpose floating structures physical modeling: state of art and new perspectives. Appl. Ocean Res. 108, 102487 https://doi.org/10.1016/j.apor.2020.102487.

Shainee, M., Ellingsen, H., Leira, B.J., Fredheim, A., 2013. Design theory in offshore fish cage designing. Aquaculture 392–395, 134–141. https://doi.org/10.1016/j.aquaculture.2013.02.016.

Tang, H., Xu, L., Hu, F., 2018. Hydrodynamic characteristics of knotted and knotless purse seine netting panels as determined in a flume tank. PLOS One 13, e0192206. https://doi.org/10.1371/journal.pone.0192206.

Theret, F., 1993. Etude de l'équilibre de surfaces réticulées placées dans le courant uniforme. Application aux chaluts. Université de Nantes,.

Tsukrov, I., Drach, A., DeCew, J., Robinson Swift, M., Celikkol, B., 2011. Characterization of geometry and normal drag coefficients of copper nets. Ocean Eng. 38, 1979–1988. https://doi.org/10.1016/j.oceaneng.2011.09.019.

Tsukrov, I., Eroshkin, O., Fredriksson, D., Swift, M.R., Celikkol, B., 2003. Finite element modeling of net panels using a consistent net element. Ocean Eng. 30, 251–270. https://doi.org/10.1016/S0029-8018(02)00021-5.

Xu, Z., Qin, H., 2020. Fluid-structure interactions of cage based aquaculture: from structures to organisms. Ocean Eng. 217, 107961 https://doi.org/10.1016/j.oceaneng.2020.107961.

Zhao, Y.-P., Li, Y.-C., Dong, G.-H., Gui, F.-K., Teng, B., 2007a. Numerical simulation of the effects of structure size ratio and mesh type on three-dimensional deformation of the fishing-net gravity cage in current. Aquac. Eng. 36, 285–301. https://doi.org/10.1016/j.aquaeng.2007.01.003.

Zhao, Y.-P., Li, Y.-C., Gui, F., Dong, G., 2007b. Numerical simulation of the effects of weight system on the hydrodynamic behavior of 3-D net of gravity cage in current. J. Hydrodyn. Ser. B 19, 442–452. https://doi.org/10.1016/S1001-6058(07)60138-3.